

Chapman University

Chapman University Digital Commons

Engineering Faculty Articles and Research

Fowler School of Engineering


5-14-2015

Portable Polarimetric Fiber Stress Sensor System for Visco-elastic and Biomimetic Material Analysis

Mark C. Harrison

Andrea M. Armani

Follow this and additional works at: https://digitalcommons.chapman.edu/engineering_articles

 Part of the [Biomaterials Commons](#), and the [Other Biomedical Engineering and Bioengineering Commons](#)

Portable Polarimetric Fiber Stress Sensor System for Visco-elastic and Biomimetic Material Analysis

Comments

This article was originally published in *Applied Physics Letters*, volume 106, issue 20, in 2015.
<https://doi.org/10.1063/1.4921243>

Copyright

American Institute of Physics

Portable polarimetric fiber stress sensor system for visco-elastic and biomimetic material analysis

Mark C. Harrison and Andrea M. Armani

Citation: [Applied Physics Letters](#) **106**, 191105 (2015); doi: 10.1063/1.4921243

View online: <http://dx.doi.org/10.1063/1.4921243>

View Table of Contents: <http://scitation.aip.org/content/aip/journal/apl/106/19?ver=pdfcov>

Published by the [AIP Publishing](#)

Articles you may be interested in

[Arrays of topographically and peptide-functionalized hydrogels for analysis of biomimetic extracellular matrix properties](#)

J. Vac. Sci. Technol. B **30**, 06F903 (2012); 10.1116/1.4762842

[Finite element calculation of residual stress in dental restorative material](#)

AIP Conf. Proc. **1459**, 312 (2012); 10.1063/1.4738480

[Research on the fiber Bragg grating sensor for the shock stress measurement](#)

Rev. Sci. Instrum. **82**, 103109 (2011); 10.1063/1.3648123

[Microfluidics-assisted photo nanoimprint lithography for the formation of cellular bioimprints](#)

J. Vac. Sci. Technol. B **28**, C6K17 (2010); 10.1116/1.3501342

[Nonlinear Viscoelastic Analysis of Uniaxial Stress-Strain Measurements of Elastomers at Constant Stretching Rates](#)

J. Rheol. **30**, 301 (1986); 10.1122/1.549850

Want to publish your paper in the
#1 MOST CITED journal in applied physics?

With *Applied Physics Letters*, you can.

AIP | Applied Physics
Letters

THERE'S POWER IN NUMBERS. Reach the world with AIP Publishing.



Portable polarimetric fiber stress sensor system for visco-elastic and biomimetic material analysis

Mark C. Harrison¹ and Andrea M. Armani^{2,a)}

¹Ming Hsieh Department of Electrical Engineering, University of Southern California, Los Angeles, California 90089, USA

²Mork Family Department of Chemical Engineering and Materials Science, University of Southern California, Los Angeles, California 90089, USA

(Received 16 April 2015; accepted 6 May 2015; published online 14 May 2015)

Non-destructive materials characterization methods have significantly changed our fundamental understanding of material behavior and have enabled predictive models to be developed. However, the majority of these efforts have focused on crystalline and metallic materials, and transitioning to biomaterials, such as tissue samples, is non-trivial, as there are strict sample handling requirements and environmental controls which prevent the use of conventional equipment. Additionally, the samples are smaller and more complex in composition. Therefore, more advanced sample analysis methods capable of operating in these environments are needed. In the present work, we demonstrate an all-fiber-based material analysis system based on optical polarimetry. Unlike previous polarimetric systems which relied on free-space components, our method combines an in-line polarizer, polarization-maintaining fiber, and a polarimeter to measure the arbitrary polarization state of the output, eliminating all free-space elements. Additionally, we develop a more generalized theoretical analysis which allows more information about the polarization state to be obtained via the polarimeter. We experimentally verify our system using a series of elastomer samples made from polydimethylsiloxane (PDMS), a commonly used biomimetic material. By adjusting the base:curing agent ratio of the PDMS, we controllably tune the Young's modulus of the samples to span over an order of magnitude. The measured results are in good agreement with those obtained using a conventional load-frame system. Our fiber-based polarimetric stress sensor shows promise for use as a simple research tool that is portable and suitable for a wide variety of applications.

© 2015 AIP Publishing LLC. [<http://dx.doi.org/10.1063/1.4921243>]

Non-destructive and rapid materials characterization methods have greatly expanded our understanding of fundamental materials behavior, and this knowledge has found numerous applications throughout society.¹ For example, a material's mechanical properties, such as the Young's modulus, degrade over time and can be used as a predictive indicator or marker of failure. Therefore, by combining failure analysis with mechanical deformation diagnostic measurements, the remaining lifetime of key aircraft components such as helicopter blades can be predicted, allowing preventive maintenance to be performed.² Recently, this type of analysis has been translated to the bio-domain and applied to more visco-elastic materials.^{3,4} These types of materials exhibit significantly different mechanical behaviors and have more complex sample handling requirements; for example, experiments with human tissue samples need to be performed in biosafety cabinets. Given these types of regulations, the conventional measurement instrumentation (a load-frame or load cell) is no longer suitable. Therefore, researchers are increasingly turning to alternative methods, such as nanoindentation, atomic force microscopy (AFM), and sonoelastography, to solve these challenges.⁵⁻⁷ In previous work, these techniques have successfully characterized the Young's modulus of biomimetic samples and of tissue.^{8,9} However, these

methods all face unique hurdles: nanoindentation generates results which require complex analysis and it has a large footprint, AFM is extremely sensitive to environmental vibrations, and sonoelastography requires manual, uncontrolled compression for signal generation. Therefore, a new system is needed which: (1) has a small footprint suitable for biosafety cabinet operation, (2) maintains high sensitivity, (3) uses disposable or sterile sensors, and (4) analyzes samples non-destructively and quickly.

The most straightforward approach for meeting these requirements is to reduce the number of components. One promising method is based on optical fiber sensors; in particular, optical sensors based on polarization-maintaining (PM) optical fiber.¹⁰ This method meets the requirements for disposability, non-destructive, and rapid analysis. In addition, these devices have a high tolerance to environmental noise, and the theoretical sensitivity is comparable. However, despite their strengths, previous work with polarimetric stress and pressure sensors has typically required free-space optical components, such as polarizers, which require alignment and are not portable.^{11,12} Additionally, these systems relied on an analyzer to probe the polarization state of the fiber at the output. This method reduces the amount of information that can be obtained from these types of sensors, limiting the overall utility. By addressing these weaknesses, a truly compact and portable polarimetric stress sensor can be created.

^{a)}Author to whom correspondence should be addressed. Electronic mail: armani@usc.edu

In the present work, we have solved these challenges by creating an all-optical fiber sensor system. Specifically, we replace all free-space components with in-line fiber counterparts and use a polarimeter to measure the arbitrary polarization state of the output light, which increases the information obtained. This combination of changes eliminates the need for any alignment. Given the increase in information, we also expand upon and generalize the previous theoretical algorithm for analyzing polarimetric sensors.^{11,13} The combination of these improvements results in a portable, adaptable, and simple-to-use all optical fiber based sensing platform.

The theoretical mechanism which enables PM-fiber based stress sensing is based on the photo-elastic effect. When stress is applied to the PM fiber, the beat length of the stressed section will change, and the fast and slow axes of the fiber will undergo a rotation of angle ϕ (Figure 1). Following the same analysis as in Chua *et al.*,¹³ we consider a two-dimensional cross-section of the stressed fiber that is acted upon by a force f [N/m] at an angle α with respect to the fast and slow axis coordinate system of the fiber. The equations governing a normalized force F , ϕ , and the stressed beat length (L_b) for a given force f [N/m] are given below

$$F = 2N^3(1 + \sigma)(p_{12} - p_{11})L_{b0}f/(\lambda\pi bY), \quad (1)$$

$$\tan(2\phi) = F \sin(2\alpha)/(1 + F \cos(2\alpha)), \quad (2)$$

$$L_b = L_{b0}(1 + F^2 + 2F \cos(2\alpha))^{-1/2}. \quad (3)$$

In these equations, σ is Poisson's ratio for the fiber, L_{b0} is the unstressed beat length, p_{ij} are photoelastic constants, Y is the Young's modulus of the fiber, and b is the radius of the fiber cladding, in meters. Additionally, the refractive indices of the fiber fast and slow axis are given by N and $N + \Delta N_0$, and ΔN_0 is related to L_{b0} , by the equation $\Delta N_0 = \lambda/L_{b0}$, where λ is the free space wavelength. Based on our system, we used the following values: $Y = 7.3 \times 10^{10}$ N/m², $\sigma = 0.17$, $b = 62.5$ μ m, $N = 1.46$, $L_{b0} = 2$ mm, $p_{11} = 0.121$, and $p_{12} = 0.27$.¹³

Figure 1 shows a diagram of the various transformations the polarized light undergoes as it travels through the experimental setup, including the rotation ϕ caused by an applied force. By tracking the various transformations the light

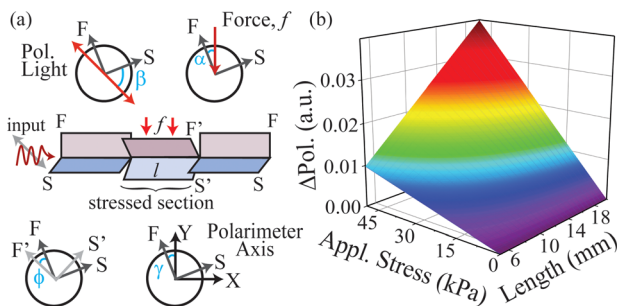


FIG. 1. Schematic diagram defining the angles used in our analysis as light propagates through the system while it interacts with the sample. The angle α is the angle between the applied force and the fast and slow axes of the fiber, β is the angle between the polarized light and the fast and slow axes of the PM fiber, γ is the angle between the fast and slow axes of the fiber and the polarimeter axes, and ϕ is the angle of rotation of the fast and slow axes when stress is applied to the fiber.

undergoes, we can determine what its polarization state will be at the output by building a series of transfer matrices

$$\begin{aligned} \begin{bmatrix} E_x \\ E_y \end{bmatrix} &= \begin{bmatrix} \cos \gamma & \sin \gamma \\ -\sin \gamma & \cos \gamma \end{bmatrix} \begin{bmatrix} 1 & 0 \\ 0 & e^{i\delta} \end{bmatrix} \begin{bmatrix} \cos \phi & -\sin \phi \\ \sin \phi & \cos \phi \end{bmatrix} \\ &\times \begin{bmatrix} e^{-jkN_s l} & 0 \\ 0 & e^{-jkN_f l} \end{bmatrix} \begin{bmatrix} \cos \phi & \sin \phi \\ -\sin \phi & \cos \phi \end{bmatrix} \\ &\times \begin{bmatrix} \cos \beta & \sin \beta \\ -\sin \beta & \cos \beta \end{bmatrix} \begin{bmatrix} E_{x0} \\ 0 \end{bmatrix}. \end{aligned} \quad (4)$$

In this equation, E_x and E_y are the x and y components of the electric field when the light reaches the polarimeter, and E_{x0} is the initial state of polarization, with the light completely polarized in the x direction. We will start with polarized light exiting the in-line polarizer and entering the PM fiber that acts as the transducer element. The polarized light is at an angle β with respect to the fast and slow axes of the PM fiber. When the light reaches the stressed section of fiber, the fast and slow axes are further rotated by an angle ϕ . In the stressed section, the light accumulates phase based on the length, l , of the stressed section and the new values of the fast and slow axis, N_f and N_s , which are related to the stressed beat length by $N_s - N_f = 2\pi/kL_b$. Upon exiting the stressed section, the light is rotated by an angle $-\phi$ to the original fast and slow axes of the PM fiber. Finally, the axes of the PM fiber may be rotated at an angle γ with respect to the x and y axes of the polarimeter.

There is one extra aspect of the transfer matrix which has not yet been accounted for. Since the polarized light is entering the PM fiber mis-aligned with the fast and slow axes, it will accumulate phase before and after the stressed section. The phase it accumulates in these sections will be related to the unstressed beat length, L_{b0} , and the effect will look similar to the matrix which accounts for accumulated phase in the stressed section. However, to account for this phase in the same way would require an accurate measurement of the entire length of fiber, which may be difficult under certain circumstances. In an effort to reduce the complexity of the testing setup, the extra phase from before and after the stressed section has been rolled into one variable, δ . This removes any difficulties in determining the phase to the fitting algorithm which is used to calibrate our sensor using experimental data and the theoretical equations above. Removing the need to know the exact length of the fiber makes the sensor a more versatile tool and reduces the complexity of the measurement.

A diagram of the testing setup used is shown in Fig. 2(a). Light from a 980 nm or 1550 nm reference laser is coupled into an in-line fiber polarizer, which is in turn connected to a length of PM fiber. The PM fiber is placed under the sample under test and secured to the compression stage of an industrial load-frame (Instron) using tape. Finally, the PM fiber output is connected to a polarimeter, where the polarization state of the light is measured as stress is applied to the sample by the Instron load-frame (Figures 2(b) and 2(c)). The arbitrary polarization state measured by the polarimeter is mathematically converted to a single variable which represents the change in polarization state.¹⁴ Simultaneously, the Instron load-frame measures the stress and strain of the sample,

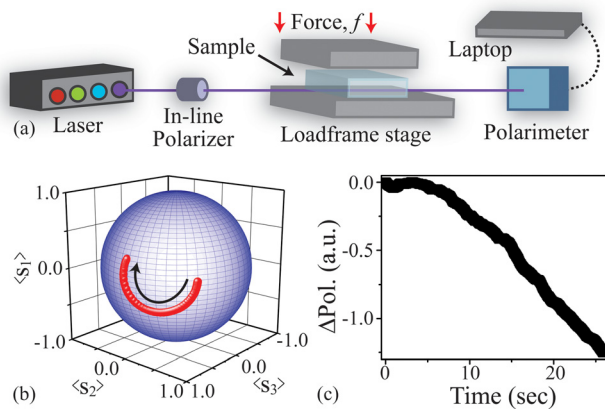


FIG. 2. (a) Schematic diagram of the testing setup. A CW laser is connected to an in-line polarizer which is in turn connected to a length of PM fiber acting as the transducing element. The PM fiber is connected to a polarimeter, which is connected to a computer for data logging. The sample is placed directly on top of the fiber and is compressed by an industrial load frame, which simultaneously measures reference data. (b) Plot of raw data from the polarimeter on a Poincaré sphere. The arrow indicates how the polarization changes as stress is applied to the fiber. (c) Plot of change in polarization vs. time of the same raw data shown in part (b) after the polarization state has been analyzed to produce a single variable representing the change in polarization state.

serving as a reference measurement. The crosshead of the load-frame moves at a velocity of 0.1 mm/s during compression. In between the sample and the sample stage, a small amount of oil is added to reduce barreling of the sample which can distort the measurement.

The raw data are in the form of a polarization state versus time curve and must be calibrated to create a stress-strain curve. In the present work, calibration curves were generated after testing to create stress-strain curves for each run, and this conversion is done using the Instron reference data and the transfer matrix detailed above to create a fitting algorithm. The algorithm fits a theoretical polarization versus force curve to the measured data by finding optimized best-fit values for α , β , γ , and δ given a wavelength (λ) and interaction length (l). Specifically, the fitting algorithm utilizes the initial and final polarization states of the experimental data, and also requires knowledge of force required to create the final polarization state. While this force can be attained from the reference data, it can also be obtained by placing a free weight on top of the sample under test. Once a best-fit has been generated, it is used to make a calibration curve.

The calibration curve is specific for a given set-up configuration. Exchanging samples causes α to vary slightly, requiring a new calibration curve to be taken. However, (β, γ, δ) will not change unless the entire system is moved. These types of initial calibration measurements are frequently performed in many fields.

To verify the ability of the system to characterize the mechanical properties of visco-elastic materials, we test our sensor using six different polydimethylsiloxane (PDMS) base:curing agent ratios spanning from 5:1 to 30:1. This range spans over an order of magnitude in Young's Modulus values and overlaps with common biomaterials such as tissue.^{6,9} The PDMS samples are prepared using the procedures recommended by the manufacturer and cut into roughly 18 mm \times 18 mm \times 5 mm rectangular samples. This sample

size fits completely under the Instron sample stage. For each base:curing agent ratio, we perform ten successive tests and measured the results using our sensor and an Instron industrial loadframe simultaneously. As such, the load-frame provides an ideal reference or control measurement. Before performing any measurements, the force on the sample is pre-loaded slightly to ensure uniform contact between the sample and the fiber. The sample is not moved, and the setup was not disturbed between each of the ten tests. Additionally, to establish the background noise level, measurements are taken with the sensor system set up on the Instron load-frame with no sample and no compression. Complementary noise measurements are also taken with the system located on an optical table.

Using different sample sets, we test with both the 980 nm and the 1550 nm lasers to investigate the wavelength-dependent response. Each wavelength offers its own advantages and disadvantages. At shorter wavelengths of light, the sensor should offer greater sensitivity, since more wavelengths will fit in to the same interaction length. This advantage is somewhat confounded by the fact that the sensitivity will vary slightly each time the sensor is set up, since it depends on specific angles in the setup, notably α . We can solve this issue by considering a case where all relevant variables ($\alpha, \beta, \gamma, \delta, l$) are the same. In this case, we calculated that the shorter wavelength, 980 nm, is slightly more sensitive to the applied force, f [N/m]. However, this assumes the same cross-sectional area of the fiber. In reality, the radius of the 1550 nm fiber is larger than the 980 nm (400 μ m as compared to 245 μ m). As such, for the same stress, the 1550 nm fiber will experience higher force than the 980 nm fiber. Therefore, when taking these two factors into consideration, the net effect is very similar sensitivity for both wavelengths, but warrants further experimental study.

Because PDMS is a visco-elastic material, the stress-strain curve is no longer linear.¹⁵ Therefore, to determine the Young's modulus, the standard method is to fit the curve to a 3rd-order polynomial and take the derivative at a defined strain. For the present series of measurements, we fit the reference and the fiber sensor stress-strain curves and took the derivative of the polynomial fit at 30% strain.

Fig. 3 shows representative experimental measurements for a pair of 25:1 PDMS samples of approximately the same size characterized using the 980 nm and 1550 nm lasers.

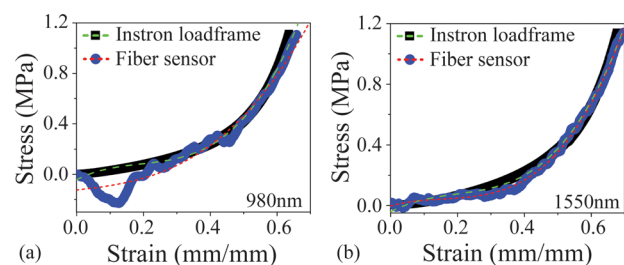


FIG. 3. Stress-strain curves for a 25:1 base:curing agent PDMS sample measured with (a) 980 nm and (b) 1550 nm laser and PM fiber. The trace of black squares is data that were measured from an Instron industrial load frame. The trace of blue circles is data that were measured simultaneously using our fiber-based sensor. 3rd-order polynomial fits are shown in green and red dashed lines, respectively. Despite some noise, there is very good agreement between both curves.

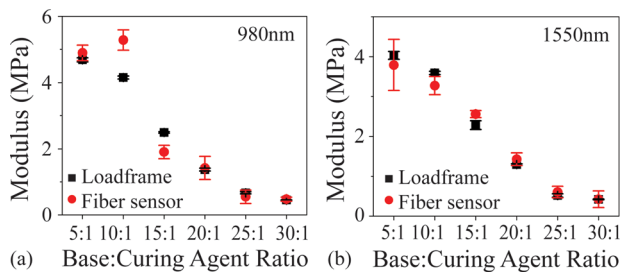


FIG. 4. Calculated Young's modulus values from the load-frame measurements and the fiber sensor data taken at both (a) 980 nm and (b) 1550 nm. The calculated values from self-consistent runs are averaged and are given here with their standard deviation.

The polarimetric sensor results are overlaid on the load-frame reference results, and the polynomial fits are shown as dashed lines. Qualitatively, there is clearly good agreement over most of the measurement range, even for this highly elastic material. A small deviation is visible for low strain values of the 980 nm graph (Fig. 3(a)). This deviation is most likely due to the sample moving slightly in the oil which is required to reduce barreling. This artifact is commonly observed with highly visco-elastic materials. However, because the Young's Modulus is determined based on a fit to the entire data set, noise at low strain does not significantly impact the overall measurement results.

To quantitatively compare the two measurement methods at the different wavelengths, the Young's moduli are determined from fits to both sets of data at 30% strain and the values from all base:curing agent ratios are plotted in Figure 4. The values in this figure are averaged from several measurements taken from the same sample and shown with their standard deviation as error bars, indicating good repeatability in our measurements. Additionally, the control measurements using the load-frame are plotted. From these plots, several key observations can be made. First, there is excellent agreement between the load-frame and the fiber sensor. Second, the deviation within a single data set is extremely low for both the load-frame and the fiber sensor. This agreement and accuracy are particularly notable given the reduction in complexity and footprint of the fiber sensor as compared to the load-frame.

To determine the ultimate theoretical sensitivity of our device, it is first necessary to determine the base noise limit. There are two possible noise sources: (1) optical noise inherent in the set-up and (2) movement of the fiber due to environmental vibrations. To thoroughly study the latter, we characterized our system's performance in four different environments: (1) a countertop in a standard synthetic chemistry lab, (2) inside of a laminar flowhood, which mimics a biosafety cabinet, (3) on an optical table, and (4) in the materials analysis lab. For all environments, we calculate the theoretical sensitivity in the form of minimum detectable stress and minimum polarization change. The results from these measurements are given in Table I. Several trends are immediately apparent. When comparing across wavelengths, the noise is consistently lower at 1550 nm than 980 nm.

When comparing across environments, the materials analysis lab was the noisiest environment, and therefore represents a good worst-case scenario for operating the sensor.

TABLE I. Noise levels given in ΔPol for different wavelengths and measuring environments.

Location	ΔPol		Stress (kPa)	
	980 nm	1550 nm	980 nm	1550 nm
Mat. Analysis Lab	0.02073	0.01606	30	23
Countertop	0.01814	0.01189	26	17
Flowhood	0.007	0.00423	10	6
Optical table	0.00333	0.00303	5	4

This finding is not surprising as the load-frame is adjacent to other mechanical testing equipment in a multi-user materials analysis lab, and this equipment is continuously in use. Therefore, the environmental vibrations in this facility are extremely high. The noise level was lower for the countertop and flowhood, and was lowest on the vibration-isolating optical table. Interestingly, the noise in the laminar flowhood was lower than the noise level on the countertop and materials analysis lab. Although one might expect that the constant airflow of the flowhood would add environmental vibration and cause movement of the fiber, it seems to have stabilized the fiber instead, causing less movement. However, it is important to note that even in the worst-case scenario, the sensor is still sensitive enough to characterize biomaterials.

In conclusion, we have demonstrated a non-destructive fiber-based polarimetric stress sensor system which utilizes a more generalized theoretical analysis to reduce complexity in the experimental setup. The sensor shows good sensitivity, low noise, and is able to accurately characterize the Young's modulus of visco-elastic or biomimetic materials after a simple calibration process. This flexible tool will be valuable to researchers for characterizing various deformable samples, such as tissue,^{4,5} when a portable, easy-to-use tool is necessary.

The authors thank Professor Steven Nutt and Zachary Melrose for use of the Instron load-frame, and Professor Michael Kassner for helpful discussions regarding the mechanical behavior of visco-elastic materials. This work was supported by the Office of Naval Research [N00014-11-1-0910], National Institutes of Health through the NIH Director's New Innovator Award Program [1DP2OD007391-01], and the National Defense Science and Engineering Graduate Research Fellowship Program.

¹F. Cellini, S. Khapli, S. D. Peterson, and M. Porfiri, *Appl. Phys. Lett.* **105**(6), 061907 (2014); H. Zhou, H. Zhang, Y. Pei, H.-S. Chen, H. Zhao, and D. Fang, *ibid.* **106**, 081904 (2015); H. Fu, S. Xu, R. Xu, J. Jiang, Y. Zhang, J. A. Rogers, and Y. Huang, *ibid.* **106**, 091902 (2015).

²G. J. Kacprzynski, A. Sarlashkar, M. J. Roemer, A. Hess, and W. Hardman, *JOM* **56**(3), 29 (2004).

³K. Hoyt, B. Castaneda, M. Zhang, P. Nigwekar, P. A. di Sant'Agnes, J. V. Joseph, J. Strang, D. J. Rubens, and K. J. Parker, *Cancer Biomarkers* **4**(4-5), 213 (2008); I. D. Johnston, D. K. McCluskey, C. K. L. Tan, and M. C. Tracey, *J. Micromech. Microeng.* **24**(3), 035017 (2014); N. S. Lu, C. Lu, S. X. Yang, and J. Rogers, *Adv. Funct. Mater.* **22**(19), 4044 (2012).

⁴T. A. Krouskop, T. M. Wheeler, F. Kallel, B. S. Garra, and T. Hall, *Ultrason. Imaging* **20**(4), 260 (1998).

⁵A. Samani, J. Bishop, C. Luginbuhl, and D. B. Plewes, *Phys. Med. Biol.* **48**(14), 2183 (2003).

⁶A. Samani, J. Zubovits, and D. Plewes, *Phys. Med. Biol.* **52**(6), 1565 (2007).

- ⁷P. N. T. Wells and H. D. Liang, *J. R. Soc. Interface* **8**(64), 1521 (2011); U. Zaleska-Dorobisz, K. Kaczorowski, A. Pawlus, A. Puchalska, and M. Inglot, *Adv. Clin. Exp. Med.* **23**(4), 645 (2014); L. Penuela, F. Wolf, R. Raiteri, D. Wendt, I. Martin, and A. Barbero, *J. Biomech.* **47**(9), 2157 (2014); M. Horimizu, T. Kawase, T. Tanaka, K. Okuda, M. Nagata, D. M. Burns, and H. Yoshie, *Micron* **48**, 1 (2013).
- ⁸B. S. Garra, *Ultrasound Quarterly* **23**(4), 255 (2007); D. W. Good, A. Khan, S. Hammer, P. Scanlan, W. M. Shu, S. Phipps, S. H. Parson, G. D. Stewart, R. Reuben, and S. A. McNeill, *Plos One* **9**(11), e112872 (2014); S. R. Mousavi, A. Sadeghi-Naini, G. J. Czarnota, and A. Samani, *Med. Phys.* **41**(3), 033501 (2014); J. Ophir, I. Cespedes, H. Ponnekanti, Y. Yazdi, and X. Li, *Ultrason. Imaging* **13**(2), 111 (1991); B. M. Ahn, J. Kim, L. Ian, K. H. Rha, and H. J. Kim, *Urology* **76**(4), 1007 (2010).
- ⁹D. W. Good, G. D. Stewart, S. Hammer, P. Scanlan, W. Shu, S. Phipps, R. Reuben, and A. S. McNeill, *Bju Int.* **113**(4), 523 (2014).
- ¹⁰J. Calero, S. P. Wu, C. Pope, S. L. Chuang, and J. P. Murtha, *J. Lightwave Technol.* **12**(6), 1081 (1994); T. K. Noh, U. C. Ryu, and Y. W. Lee, *Sens. Actuators A* **213**, 89 (2014); Y. Verbandt, B. Verwilghen, P. Cloetens, L. VanKempen, H. Thienpont, I. Veretennicoff, G. VanVinckenroy, W. P. DeWilde, and M. R. H. Voet, *Opt. Rev.* **4**(1A), A75 (1997).
- ¹¹R. C. Gauthier and J. Dhliwayo, *Opt. Laser Technol.* **24**(3), 139 (1992); G. Liu and S. L. Chuang, *Sens. Actuators A* **69**(2), 143 (1998).
- ¹²V. M. Murukeshan, P. Y. Chan, L. S. Ong, and A. Asundi, *Sens. Actuators A* **80**(3), 249 (2000).
- ¹³T. H. Chua and C. L. Chen, *Appl. Opt.* **28**(15), 3158 (1989).
- ¹⁴See supplementary material at <http://dx.doi.org/10.1063/1.4921243> for additional details.
- ¹⁵I. K. Lin, K.-S. Ou, Y.-M. Liao, Y. Liu, K.-S. Chen, and X. Zhang, *J. Microelectromech. Syst.* **18**(5), 1087 (2009); A. Mata, A. J. Fleischman, and S. Roy, *Biomed. Microdev.* **7**(4), 281 (2005).